Early Bone Healing and Biomechanical Fixation of Dual Acid-Etched and As-Machined Implants with Healing Chambers: An Experimental Study in Dogs

Estevam A. Bonfante, DDS, MS, PhD[1]/Rodrigo Granato, DDS, MS[2]/
Charles Marin, DDS, MS[2]/Marcelo Suzuki, DDS[3]/Sergio R. Oliveira, DDS, MS, PhD[4]/
Gabriela Giro, DDS, MS[5]/Paulo G. Coelho, DDS, MS, BS, MSMtE, PhD[6]

Purpose: *To evaluate the biomechanical fixation, bone-to-implant contact (BIC), and bone morphology of screw-type root-form implants with healing chambers with as-machined or dual acid-etched (DAE) surfaces in a canine model.* ***Materials and Methods:*** *The animal model included the placement of machined (n = 24) and DAE (n = 24) implants along the proximal tibiae of six mongrel dogs, which remained in place for 2 or 4 weeks. Following euthanasia, half of the specimens were subjected to biomechanical testing (torque to interface failure) and the other half were processed for histomorphologic and histomorphometric (%BIC) assessments. Statistical analyses were performed by one-way analysis of variance at the 95% confidence level and the Tukey post hoc test for multiple comparisons.* ***Results:*** *At 4 weeks, the DAE surface presented significantly higher mean values for torque to interface failure overall. A significant increase in %BIC values occurred for both groups over time. For both groups, bone formation through the classic appositional healing pathway was observed in regions where intimate contact between the implant and the osteotomy walls occurred immediately after implantation. Where contact-free spaces existed after implantation (healing chambers), an intramembranous-like healing mode with newly formed woven bone prevailed.* ***Conclusions:*** *In the present short-term evaluation, no differences were observed in BIC between groups; however, an increase in biomechanical fixation was seen from 2 to 4 weeks with the DAE surface.* Int J Oral Maxillofac Implants 2011;26:75–82

Key words: *animal study, bone-to-implant contact, dental implants, implant design, surface properties, torque*

[1]PhD Candidate, Department of Prosthodontics, University of São Paulo, Bauru School of Dentistry, Bauru, Brazil.
[2]PhD Candidate, Department of Dentistry, Universidade Federal de Santa Catarina, Florianopolis, Brazil.
[3]Assistant Professor, Department of Prosthodontics, Tufts University School of Dental Medicine, Boston, Massachusetts.
[4]Assistant Professor, Department of Periodontology, Universidade Federal de Uberlandia, Uberlandia, Brazil.
[5]PhD Candidate, Department of Oral Diagnosis and Surgery, Faculdade de Odontologia de Araraquara, São Paulo State University, Araraquara, São Paulo, Brazil.
[6]Assistant Professor, Department of Biomaterials and Biomimetics, New York University, New York, New York.

Correspondence to: Dr Estevam Bonfante, Al. Octávio Pinheiro Brisola, 9-75, Bauru, SP, Brasil, 17012-901. Fax: +55-14-32342566. Email: estevamab@gmail.com

Following the seminal publication by Brånemark's group in 1969[1] and the definition of osseointegration as the close contact between bone and biomaterials at the microscopic level,[2,3] many manufacturing, laboratory, and clinical developments have expanded the application of dental implants.[4] According to the treatment modality established in the early 1980s, a strictly controlled surgical placement of biocompatible titanium screws was followed by a latency period of several months where the absence of occlusal functional loading was demanded to allow bone healing and, hence, device osseointegration.[1] Verification of implant osseointegration was assured in a second surgical procedure, followed by a series of prosthetic clinical and laboratory steps that resulted in the re-establishment of function and esthetics.[5–7]

The application of the aforementioned classical two-stage protocol has been extensively documented during the last 40 years, and success rates above 90% in controlled clinical trials have rendered implant dentistry a successful and safe treatment modality.[6,8,9] Despite the high success rates, implant design parameters have changed over time, and the quest for decreased treatment time has spurred implant design research. A variety of methods have been used in an attempt to enhance bone healing after device implantation, including bulk device design,[10] additions of biologic compounds,[11] and biomaterial surface modifications.[10–18] Because the implant surface is the first component to interact with the host, several surface modifications, including surface texturing, have been extensively investigated in the search for improved bone healing that would allow immediate or early loading of dental implants.[4] From an early healing standpoint, histomorphometric and biomechanical studies have shown an improved osteogenic response with acid-etched and/or grit-blasted microtextured surfaces (average R_a ranging from 0.5 to 2.0 μm) versus as-machined dental implant surfaces.[2,3,19]

Implant macro design has also been investigated. A recent study of the bone healing kinetics around implants of a screw-type root-form design and those of a bulk design that allowed void spaces between the implant bulk and the osteotomy walls showed bone-to-implant contact (BIC) and bone area fraction occupancy progressing in parallel along study time frames, with a significant effect of time for both implant macro designs.[20]

Regarding implant designs that allow for healing chambers (unlike root-form protocols, where the osteotomy dimensions allow for intimate contact between its walls and the implant surface), a number of studies[12,21–25] have provided histologic evidence of prominent woven bone formation and maturation within experimental wound chambers cut into the implant bulk. However, despite rapid woven bone filling, pure healing-chamber designs result in almost no primary stability.[20] In an attempt to improve on this circumstance, several investigators have employed either *(1)* experimental implant designs with an outer thread design that provided stability while the inner thread and osteotomy dimensions included healing chambers[21–23] or *(2)* alterations in osteotomy dimensions in large thread-pitch implant designs.[24] Among these, only one study has evaluated the mechanical stability of a threaded implant with healing chambers on two surfaces through resonance frequency analysis.[23] Thus, while promising results have been obtained with screw-type implant designs with healing chambers, further biomechanical characterization of such an implant configuration is desirable. Given the statistical robustness of data available in the literature concerning as-machined surfaces,[26] the present investigation considered the machined surface as a control in an attempt to more precisely understand the effect of a rougher surface on selected osseointegration parameters. This study was designed to evaluate the torque to interface failure, BIC, and bone morphology for as-machined and dual acid-etched (DAE) surfaces in screw-type root-form implants provided with healing chambers.

MATERIALS AND METHODS

This study used an experimental screw-type root-form grade 5 Ti alloy endosseous implant (Unitite, SIN). It was 4 mm in diameter and 10 mm in length and had microthreads on the cervical third and two distinct thread patterns through its remaining length (Fig 1). Two implant surfaces were examined: as-machined and DAE (n = 24 for each surface).

Animal Model

For the animal model, 24 implants of each surface were utilized. Six adult male mongrel dogs, each about 1.5 years old, were acquired following the approval of the Ethics Committee for Animal Research at Universidade Federal de Santa Catarina, Brazil. Prior to and following surgical procedures, the animals were not constrained and were allowed to move within their cages.

Prior to general anesthesia, atropine sulfate (0.044 mg/kg) and xylazine chlorate (8 mg/kg) were administered intramuscularly. A 15 mg/kg dose of ketamine chlorate was then used to achieve general anesthesia.

The surgical site for implant placement was the proximal tibia (the left and right limbs provided specimens that remained 2 and 4 weeks in vivo, respectively), which was initially shaved with a razor blade. After antiseptic iodine solution was applied, an incision through the skin, about 5 cm in length, was made for access to the periosteum, which was elevated for bone exposure.

For implant placement, a 2-mm-diameter pilot drill at 1,200 rpm under abundant saline irrigation was used for initial socket drilling. Then, sequential drilling with a 3.0-mm cylindric bur was performed at 800 rpm, followed by a final bur with dimensions according to the schematic representation shown in Fig 1. The implants were then inserted in the osteotomy at a torque of 45 Ncm per the manufacturer's recommendation. The first implant was inserted 2 cm below the joint capsule line at the central mediolateral position of the proximal tibia. The other three implants were placed in the distal direction, 1 cm apart, along the

central region of the bone. Balanced surgical procedures were used to allow comparison of the torque and histology of the same number of implant surfaces with regard to time in vivo, limb, surgical site (1 through 4), and animal.

Following implant placement, a healing cap was attached to each internal-hex implant to prevent tissue overgrowth. The soft tissue was sutured in layers following standard procedures: the periosteum was sutured with Vicryl 4-0 (Ethicon/Johnson & Johnson) and the skin was closed with 4-0 nylon (Ethicon/Johnson & Johnson).

Postoperative antibiotic and anti-inflammatory medication included a single dose of benzylpenicillin benzatine (20,000 IU/kg) intramuscularly and ketoprofen 1% (1 mL/5 kg). The animals were euthanized after 2 and 4 weeks by anesthesia overdose, and the upper third of each tibia was retrieved by sharp dissection. Half of the specimens were used for mechanical testing, and the other half underwent nondecalcified processing for histologic and histomorphometric evaluation.

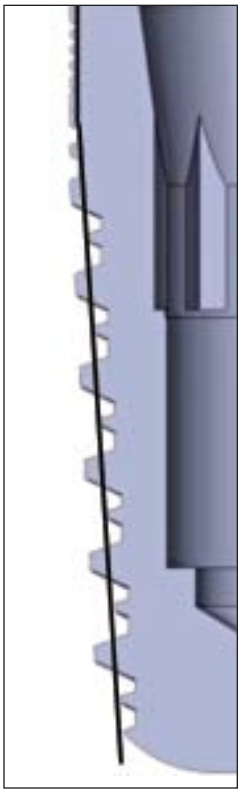

Fig 1 Two-dimensional computer-assisted design representation of the implant macrogeometry showing microthreads in the crestal region and two thread patterns along its remaining length. The line depicts the outer diameter of the final bur with respect to the implant shape, which allowed the formation of healing chambers at regions between the larger and smaller threads.

Removal Torque Testing

For torque testing, the tibia was adapted to an electronic torque machine equipped with a 2,000-Ncm torque load cell (Test Resources). Custom machined tooling was adapted to each implant's internal connection and bone blocks were positioned carefully to avoid specimen misalignment during testing. The implants were torqued counterclockwise at a rate of ~0.196 radians/minute, and a torque versus displacement curve was recorded for each specimen. The torque machine was set to automatically stop when a torque drop of 20% from the highest load was detected to minimize bone/implant interface damage.[25,27]

Histomorphometric Preparation and Examination

At necropsy, the tibiae were retrieved by sharp dissection and surgical blades were used to remove the soft tissues. The implants in bone were reduced to blocks and were then immersed in 10% buffered formalin solution for 24 hours. The blocks were then washed in running water for 24 hours and gradually dehydrated in a series of alcohol solutions ranging from 70% to 100% ethanol. Following dehydration, the samples were embedded in a methacrylate-based resin (Technovit 9100, Heraeus Kulzer) according to the manufacturer's instructions. The blocks were then cut into slices (~300-µm thickness) along the implant's long axis with a precision diamond saw (Isomet 2000, Buehler) and glued to acrylic glass plates with an acrylate-based cement; a 24-hour setting time was allowed prior to grinding and polishing. The sections were then reduced to a final thickness of ~30 µm by means of a series of silicon carbide abrasive papers (400, 600, 800, 1,200, and 2,400 grit) (Buehler) in a grinding/polishing machine (Metaserv 3000, Buehler) under water irrigation.[28] The sections were then stained with toluidine blue and observed with optical microscopy for histomorphologic evaluation.

BIC was determined at magnifications of ×50 to ×200 (Leica DM2500M, Leica Microsystems) by means of computer software (Leica Application Suite, Leica Microsystems). The regions of BIC along the implant perimeter were subtracted from the total implant perimeter, and calculations were performed to determine the %BIC.[20]

Statistical Analyses

Following normality and variance checks, statistical analyses were performed by one-way analysis of variance with BIC and torque to interface failure considered as dependent variables. The Tukey post hoc test was used for multiple comparisons. Statistical significance was indicated by *P* values less than 5%.

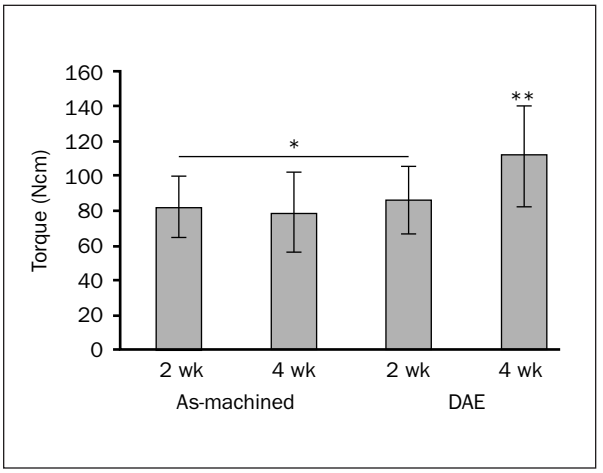

Fig 2 Torque to interface failure values (mean ± SD) showing that the DAE surface at 4 weeks presented significantly higher values than all other groups ($P < .03$). Groups with the same number of asterisks are statistically homogenous.

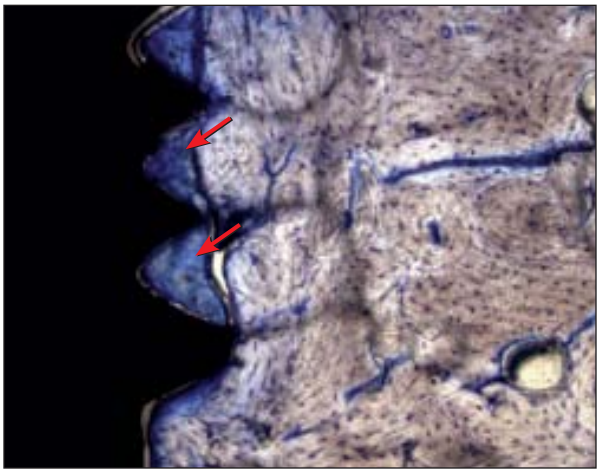

Fig 3 Regardless of implant surface, optical microscopy at the microthread region showed woven bone formation *(red arrows)* where bone had been compressed immediately after placement as early as 2 weeks after placement.

RESULTS

Animal surgical and follow-up procedures demonstrated no complications regarding procedural conditions, postoperative infection, or other clinical concerns. All implants were integrated into the bone after the 4-week healing period.

Mean values for torque to interface failure (Fig 2) were not significantly different among the machined implants at 2 and 4 weeks and the DAE implants at 2 weeks ($P > .05$). However, at 4 weeks the DAE implants presented significantly higher torque values (mean ± SD) than the as-machined group ($P < .03$).

Qualitative evaluation of the toluidine blue–stained thin sections showed intimate contact between cortical and trabecular bone (Figs 3 to 5) for both implant surfaces, including the regions that were in close proximity to (Fig 3) or further away from the osteotomy walls (Figs 4 and 5). The interplay between implant geometry and final drilling dimensions allowed intimate contact between implant and bone at the microthreads' outer diameter and the outer portion of the large threads. At the same time, healing chambers between larger and smaller threaded regions of the implant and the osteotomy walls were formed (Figs 4 and 5). All implants presented new bone formation through the classic appositional healing pathway at regions where intimate contact existed between the implant surface and bone immediately after placement. These regions comprised the microthreaded region and the outer aspects of the outer threads. In contrast, the initial healing pattern observed in the healing chambers that formed as a result of the implant design and surgical drilling followed an intramembranous-type healing mode, with the chamber partially filled with newly formed woven bone (Figs 4 and 5).

No substantial morphologic differences were observed for the different implant surfaces after 2 and 4 weeks in vivo. At 2 weeks, woven bone formation was observed in close proximity with both implant surfaces (Fig 4). At 4 weeks, replacement of the woven bone by lamellar bone was observed at both implant surfaces (Fig 5).

Specific to the healing chambers at the cortical and trabecular bone regions, woven bone formation occurred primarily at the central region of the healing chamber for the machined implants, whereas woven bone formation occurred at both central regions and at regions in close proximity to the implant surface for the DAE implants (Figs 4 and 5).

Evaluation of BIC as a function of implant surface and time revealed significant differences between groups ($P < .01$). A significant increase in %BIC occurred for both surfaces over time (Fig 6). Although the highest %BIC was recorded for the DAE surface group at 4 weeks, it did not reach statistical significance versus the machined surface at 4 weeks. The %BIC for the DAE surface at 2 and 4 weeks was not significantly different from the %BIC for the as-machined surface.

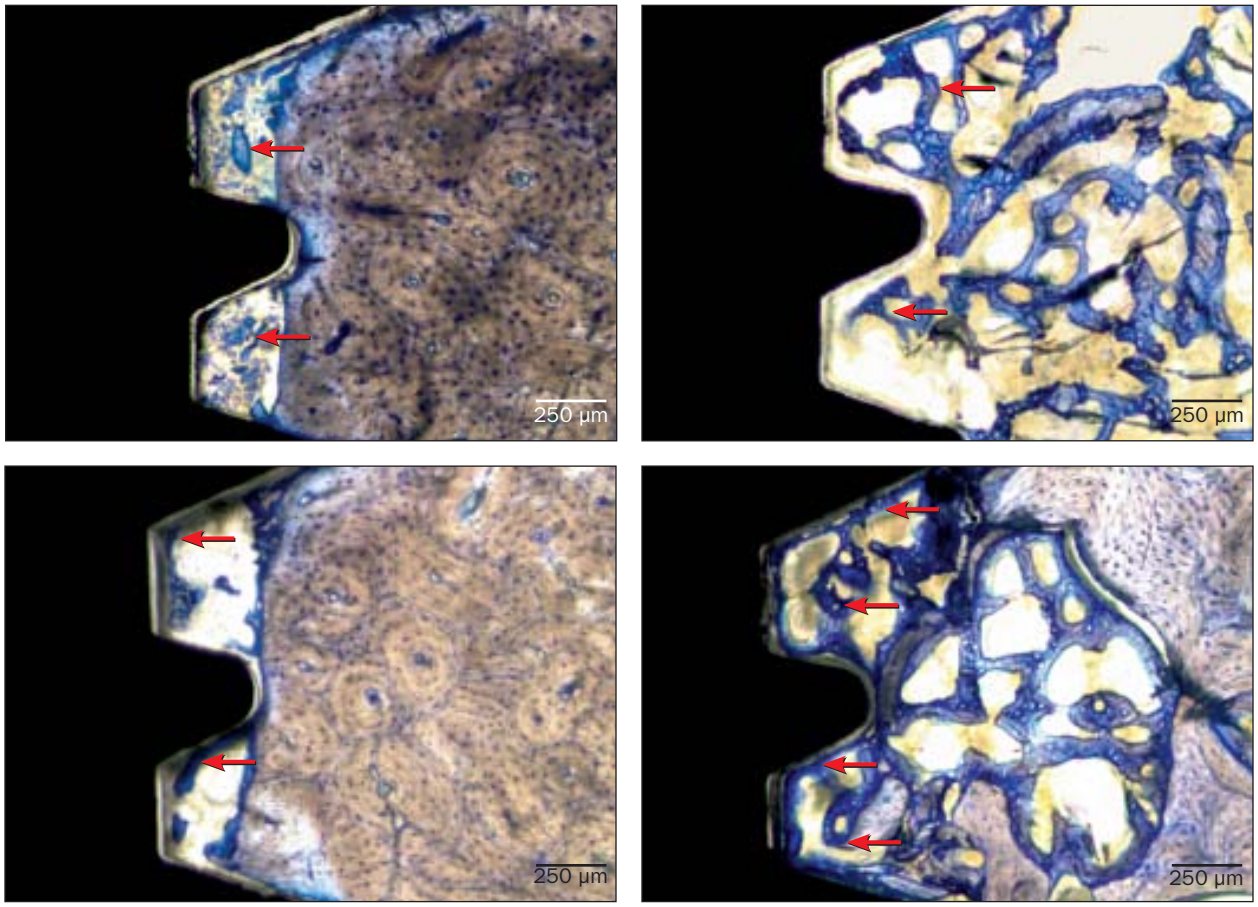

Fig 4 Optical micrographs of the bone-implant interface at 2 weeks for the as-machined surface at *(above left)* cortical and *(above right)* trabecular regions and for the DAE implant surface at 2 weeks at *(below left)* cortical and *(below right)* trabecular regions. At cortical regions, initial woven bone formation *(red arrows)* occurred primarily at the center of the healing chamber for the machined surface, whereas initial ossification occurred along the implant surface in the healing chamber region for the DAE surface. At trabecular regions, a woven bone *(red arrows)* formation pattern for the as-machined surface appeared primarily at the central regions of the healing chamber, whereas for the DAE surface it was present in both the central regions and along the implant surface.

DISCUSSION

Immediate/early loading of dental implants has long been of interest to clinicians and patients to reduce treatment times.[29–31] Efforts to refine clinical protocols, improve implant designs, and develop new implant surfaces have rendered immediate loading a well-documented and predictable procedure for selected patients, as reported in a systematic review.[32] Despite the evidence from that systematic review showing a positive influence of textured surfaces, especially in poor-quality bone,[32] the variety of implant designs and surface texturing methods found among the evaluated studies has hindered a clear understanding of the role of individual implant macroscopic and microscopic features associated with enhanced bone healing.

A recent evaluation of BIC and its correlation with resonance frequency analysis in threaded implants with healing chambers of as-machined and sand-blasted/acid-etched surfaces (SAE) placed in canine mandibles showed increasing and significantly higher BIC at early implantation times for SAE surfaces compared to as-machined surfaces. Interestingly, the resonance frequency values remained relatively unchanged for SAE and as-machined surfaces throughout the observation period.[23] In contrast, the present biomechanical tests revealed that a significant difference was found for the DAE surface at 4 weeks, which presented higher mean values for torque to interface failure when compared to the remaining observation times and groups. While similar experimental implant concepts were used in the present study and that of Abrahamsson et al,[23] comparisons should be made

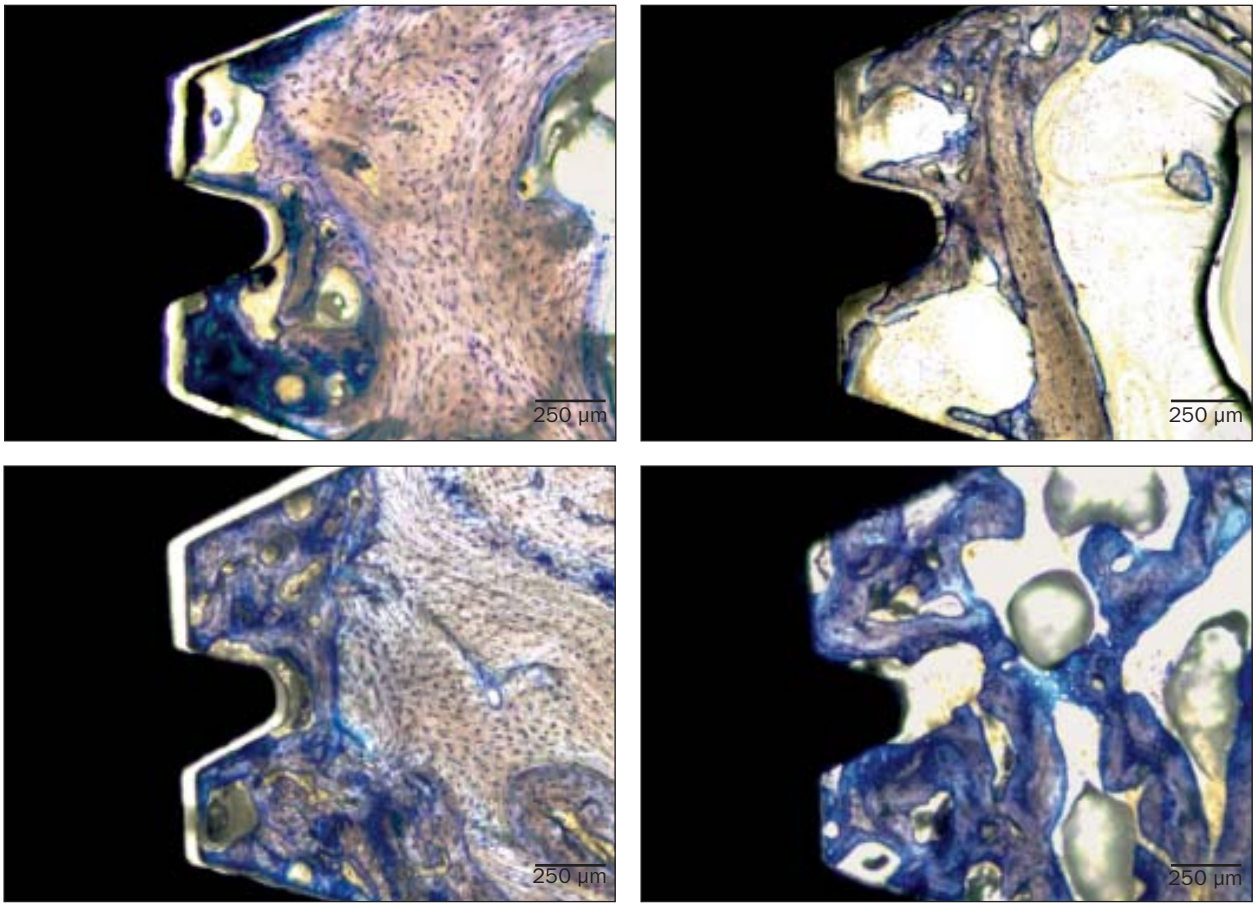

Fig 5 Optical micrographs of the bone-implant interface at 4 weeks for the as-machined surface at *(above left)* cortical and *(above right)* trabecular regions and for the DAE implant surface at 4 weeks at *(below left)* cortical and *(below right)* trabecular regions. In both the cortical and trabecular regions, replacement of woven bone by lamellar bone *(lighter staining)* was observed.

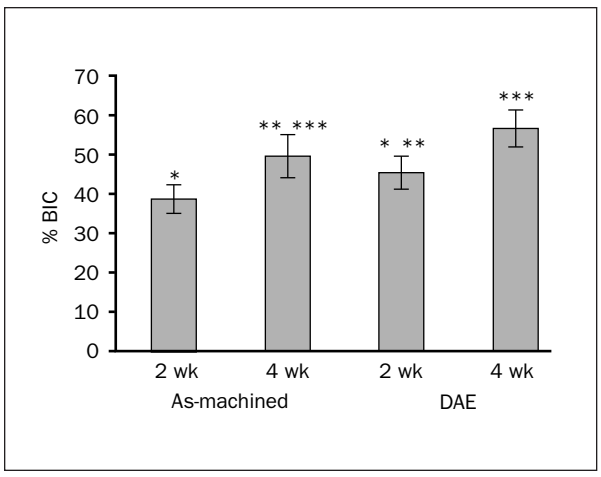

Fig 6 Significant differences were observed in BIC between different groups ($P < .01$) (means ± 95% confidence intervals). Bars with the same number of asterisks indicate statistically homogenous groups.

with caution, since Abrahamsson et al placed implants in the mandible, whereas in the present study they were in the tibia. Although it has been suggested that the greater biomechanical fixation of rougher surfaces compared to smoother surfaces was a result of mechanical interlocking between the surface and bone, nanoindentation tests showed[33] that surface microtexturization (DAE, R_a ranging from 0.5 to 1.0 µm[2,3]) resulted in improved bone mechanical properties versus as-machined surfaces (R_a also ranging from 0.5 to 1.0 µm[2,3]) at early implantation times. Regardless of the lack of significant difference between as-machined and DAE surfaces at 2 weeks, torque to interface failure for the latter was comparable to that of as-machined at 4 weeks, which remained unchanged as time in vivo elapsed.

The sequential surgical approach and implant distribution used in the present investigation resulted in the comparison of the same number of machined and DAE implants per animal, surgical site, and time

in vivo for histomorphometry and biomechanical testing. This procedure was used in an attempt to minimize bias resulting from potential differences in cortical/trabecular ratios from proximal to distal observed along the tibia.[34] Also, the tibia model provided histologic sections showing the interaction between trabecular and cortical bone and the as-machined and DAE surfaces, which was an advantage over other models in which histomorphometric and biomechanical testing may have been restricted mostly to cortical bone.[12,21] A potential limitation of the present model is the complex biomechanical scenario that evolves during healing, modeling, and remodeling, because loading occurred as the animals moved within their cages.

The histologic results showed close contact between implant and bone at the microthreads and the outer portion of the large threads, regardless of implant surface. The classic appositional healing pathway characterized bone healing in these regions. After 2 weeks, woven bone formation was observed where the bone was under compression at the microthread regions of as-machined and DAE implant surfaces.

Although no substantial morphologic differences were observed for the different implant surfaces after 2 and 4 weeks in vivo, cortical and trabecular bone regions at healing chambers showed woven bone formation occurring primarily at the central region for the machined surface, whereas woven bone formation occurred at both central regions and at regions in close proximity to the implant surface for the DAE implants. It has been demonstrated that blood clots forming between healing chambers walls and bone evolve toward a provisional matrix that includes a high content of mesenchymal cells in the connective tissue.[21,35] Thus, blood clot retention and maintenance throughout the healing chamber are desirable, and it can be speculated that the different qualitative spatial distribution observed between surfaces was caused by the roughness of the DAE surface and its ability to more evenly keep the blood clot within the chamber region.[23]

CONCLUSION

In this study in dogs, a screw-type root-form implant provided with healing chambers presented no significant difference at 4 weeks in bone-implant contact percentage values, regardless of whether the implant surface was left as-machined or dual acid-etched. The roughness of the dual acid-etched implant surface appeared to be a factor contributing, at 4 weeks, to a significantly higher torque to interface failure overall, as well as to woven bone formation at healing chambers occurring not only in central regions but also in regions in close proximity to the implant surface. Future studies including longer follow-up evaluations are warranted.

ACKNOWLEDGMENTS

This study was partially funded by the Department of Oral and Maxillofacial Surgery at Universidade Federal de Santa Catarina. The experimental implants were manufactured and provided by Sistema de Implante Nacional, SIN, Sao Paulo, Brazil.

REFERENCES

1. Brånemark PI, Adell R, Breine U, Hansson BO, Lindstrom J, Ohlsson A. Intra-osseous anchorage of dental prostheses. I. Experimental studies. Scand J Plast Reconstr Surg 1969;3:81–100.
2. Albrektsson T, Wennerberg A. Oral implant surfaces: Part 1—Review focusing on topographic and chemical properties of different surfaces and in vivo responses to them. Int J Prosthodont 2004;17:536–543.
3. Albrektsson T, Wennerberg A. Oral implant surfaces: Part 2—Review focusing on clinical knowledge of different surfaces. Int J Prosthodont 2004;17:544–564.
4. Coelho PG, Granjeiro JM, Romanos GE, et al. Basic research methods and current trends of dental implant surfaces. J Biomed Mater Res B Appl Biomater 2009;88:579–596.
5. Brånemark PI, Engstrand P, Ohrnell LO, et al. Brånemark novum: A new treatment concept for rehabilitation of the edentulous mandible. Preliminary results from a prospective clinical follow-up study. Clin Implant Dent Relat Res 1999;1:2–16.
6. Jemt T, Chai J, Harnett J, et al. A 5-year prospective multicenter follow-up report on overdentures supported by osseointegrated implants. Int J Oral Maxillofac Implants 1996;11:291–298.
7. van Steenberghe D, Lekholm U, Bolender C, et al. Applicability of osseointegrated oral implants in the rehabilitation of partial edentulism: A prospective multicenter study on 558 fixtures. Int J Oral Maxillofac Implants 1990;5:272–281.
8. Brånemark PI, Hansson BO, Adell R, et al. Osseointegrated implants in the treatment of the edentulous jaw. Experience from a 10-year period. Scand J Plast Reconstr Surg Suppl 1977;16:1–132.
9. Henry PJ, Laney WR, Jemt T, et al. Osseointegrated implants for single-tooth replacement: A prospective 5-year multicenter study. Int J Oral Maxillofac Implants 1996;11:450–455.
10. Lemons J, Dietsch-Misch F. Biomaterials for dental implants. In: Misch CE (ed). Contemporary Implant Denstistry. St Louis: Mosby, 1999:271–302.
11. Liu Y, de Groot K, Hunziker EB. Osteoinductive implants: The mise-en-scene for drug-bearing biomimetic coatings. Ann Biomed Eng 2004;32:398–406.
12. Buser D, Broggini N, Wieland M, et al. Enhanced bone apposition to a chemically modified SLA titanium surface. J Dent Res 2004;83:529–533.

13. deGroot K KC, Wolke JGC, deBieck-Hogervorst JM. Plasma-sprayed coating of calcium phosphate. In: Yamamuro T, Hench LL, Wilson J (eds). Handbook of Bioactive Ceramics. Vol II: Calcium Phosphate and Hydroxyapatite Ceramics. Boca Raton: CRC, 1990:17–25.
14. Lacefield WR. Hydroxyapatite coatings. Ann N Y Acad Sci 1988;523:72–80.
15. Lacefield WR. Current status of ceramic coatings for dental implants. Implant Dent 1998;7:315–322.
16. Ong JL, Carnes DL, Bessho K. Evaluation of titanium plasma-sprayed and plasma-sprayed hydroxyapatite implants in vivo. Biomaterials 2004;25:4601–4606.
17. Park YS, Yi KY, Lee IS, Han CH, Jung YC. The effects of ion beam-assisted deposition of hydroxyapatite on the grit-blasted surface of endosseous implants in rabbit tibiae. Int J Oral Maxillofac Implants 2005;20:31–38.
18. Yang Y, Kim KH, Ong JL. A review on calcium phosphate coatings produced using a sputtering process—An alternative to plasma spraying. Biomaterials 2005;26:327–337.
19. Albrektsson T, Brånemark PI, Hansson HA, Lindstrom J. Osseointegrated titanium implants. Requirements for ensuring a long-lasting, direct bone-to-implant anchorage in man. Acta Orthop Scand 1981;52:155–170.
20. Leonard G, Coelho PG, Polyzois I, Stassen L, Claffey N. A study of the bone healing kinetics of plateau versus screw root design titanium dental implants. Clin Oral Implants Res 2009;20:232–239.
21. Berglundh T, Abrahamsson I, Lang NP, Lindhe J. De novo alveolar bone formation adjacent to endosseous implants. Clin Oral Implants Res 2003;14:251–262.
22. Abrahamsson I, Berglundh T, Linder E, Lang NP, Lindhe J. Early bone formation adjacent to rough and turned endosseous implant surfaces. An experimental study in the dog. Clin Oral Implants Res 2004;15:381–392.
23. Abrahamsson I, Linder E, Lang NP. Implant stability in relation to osseointegration: An experimental study. Clin Oral Implants Res 2009;20:313–318.
24. Coelho PG, Suzuki M, Guimaraes MV, et al. Early bone healing around different implant bulk designs and surgical techniques: A study in dogs. Clin Implant Dent Relat Res 2010; 12:202–208.
25. Granato R, Marin C, Suzuki M, Gil JN, Janal MN, Coelho PG. Biomechanical and histomorphometric evaluation of a thin ion beam bioceramic deposition on plateau root form implants: An experimental study in dogs. J Biomed Mater Res B Appl Biomater 2009;90:396–403.
26. Albrektsson T, Jansson T, Lekholm U. Osseointegrated dental implants. Dent Clin North Am 1986;30:151–174.
27. Coelho PG, Lemons JE. Physico/chemical characterization and in vivo evaluation of nanothickness bioceramic depositions on alumina-blasted/acid-etched Ti-6Al-4V implant surfaces. J Biomed Mater Res A 2009;90:351–361.
28. Donath K, Breuner G. A method for the study of undecalcified bones and teeth with attached soft tissues. The Sage-Schliff (sawing and grinding) technique. J Oral Pathol 1982;11:318–326.
29. Becker W, Goldstein M. Immediate implant placement: Treatment planning and surgical steps for successful outcome. Periodontol 2000 2008;47:79–89.
30. Goldstein M, Boyan BD, Schwartz Z. The palatal advanced flap: A pedicle flap for primary coverage of immediately placed implants. Clin Oral Implants Res 2002;13:644–650.
31. Hammerle CH, Chen ST, Wilson TG Jr. Consensus statements and recommended clinical procedures regarding the placement of implants in extraction sockets. Int J Oral Maxillofac Implants 2004;19(suppl):26–28.
32. Del Fabbro M, Testori T, Francetti L, Taschieri S, Weinstein R. Systematic review of survival rates for immediately loaded dental implants. Int J Periodontics Restorative Dent 2006;26:249–263.
33. Butz F, Aita H, Wang CJ, Ogawa T. Harder and stiffer bone osseointegrated to roughened titanium. J Dent Res 2006;85: 560–565.
34. Marin C, Granato R, Suzuki M, Gil JN, Piattelli A, Coelho PG. Removal torque and histomorphometric evaluation of bioceramic grit-blasted/acid-etched and dual acid-etched implant surfaces: An experimental study in dogs. J Periodontol 2008;79:1942–1949.
35. Berglundh T, Abrahamsson I, Albouy JP, Lindhe J. Bone healing at implants with a fluoride-modified surface: An experimental study in dogs. Clin Oral Implants Res 2007;18:147–152.